

**Inclusive particle production at HERA:  
Higher-order QCD corrections  
to the resolved quasi-real photon contribution**

F.M. Borzumati  
B.A. Kniehl  
G. Kramer

*II. Institut für Theoretische Physik \*  
Universität Hamburg, 2000 Hamburg 50, Germany*

**Abstract**

We calculate in next-to-leading order inclusive cross sections of single-particle production via resolved photons in  $ep$  collisions at HERA. Transverse-momentum and rapidity distributions are presented and the scale dependence is studied. The results are compared with first experimental data from the H1 Collaboration at HERA.

---

\*Supported by the Bundesministerium für Forschung und Technologie, 05 5HH 91P(8), Bonn, FRG.

# 1 Introduction

The inclusive production of high-transverse-momentum single hadrons by collisions of protons and the quasi-real photons emitted by an electron beam is an interesting process for testing the QCD-improved parton model. First experimental results on this process have been presented recently by the H1 Collaboration at HERA [1]. These data have been compared already with theoretical predictions to leading order (LO) in QCD. The LO QCD formalism consists of using the tree-level results for the hard-scattering cross sections, the one-loop expression for the running coupling constant, and structure functions and fragmentation functions generated by one-loop evolution kernels. It is well known that such LO estimates suffer from normalization uncertainties due to the renormalization/factorization scale dependence. The normalization ambiguities are substantially reduced in the next-to-leading order (NLO) formalism.

There exist two distinct mechanisms which contribute to the inclusive photoproduction of hadrons at high energies. The photon can interact either directly with the partons originating from the proton, giving rise to the “direct” process, or via its quark and gluon content, the so-called “resolved” process. In both cases high- $p_T$  final partons are produced, which fragment into single hadrons with the same  $p_T$ .

Both contributions are of the same order in the perturbative expansion. The LO contribution of the resolved part is given by LO parton-parton scattering terms, multiplied by LO structure functions of the photon and proton and LO fragmentation function of the final hadron. Since the parton-parton scattering terms are of  $\mathcal{O}(\alpha_s^2)$  and the photon structure function of  $\mathcal{O}(\alpha/\alpha_s)$ , both LO contributions of the direct and resolved parts are of  $\mathcal{O}(\alpha\alpha_s)$ .

Recent data from the H1 and ZEUS Collaborations [1,2] indicate that the resolved photoproduction dominates at HERA energies, for small transverse momenta,  $p_T$ , and negative rapidities of the produced hadron relative to the laboratory system,  $y_{\text{lab}}$  (we take  $y_{\text{lab}}$  to be positive in the direction of the electron beam). So either by appropriate kinematical cuts in  $p_T$  and  $y_{\text{lab}}$  or by observing the remnants of the resolved photon near the beam pipe it should be feasible to obtain information on the resolved part alone [1]. Here it is understood that  $p_T$  is still outside the region of soft particle production, which dominates for  $p_T \lesssim 1$  GeV. Thus considering resolved photoproduction of single hadrons as a separate process, it is important to obtain quantitative predictions for it. For this purpose, we

have calculated NLO corrections, which are of  $\mathcal{O}(\alpha_s^3)$  for the parton-parton scattering process, in the case of the resolved photoproduction alone. It is clear that in the high- $p_T$  range direct and resolved photoproduction yield comparable contributions, which must be combined in order to obtain a reliable prediction. This will be left for future work.

To perform a consistent calculation of inclusive single-particle production in the NLO formalism, we need the hard-scattering cross section in NLO, with two-loop  $\alpha_s(\mu)$ , two-loop evolved structure functions of the photon and the proton, and two-loop-evolved fragmentation functions. Only in conjunction with each other are these elements unambiguously defined.

As far as the proton structure functions are concerned, NLO parametrizations exist already for some time [3,4,5]. As for the photon structure functions, recently three NLO sets of parametrizations have appeared in the literature [6,7,8]. They have been tested against the available experimental data on the photon structure function  $\mathcal{F}_2^\gamma(x, Q^2)$ .

Unfortunately, such analyses do not exist for the fragmentation functions of quarks and gluons in general. Only the  $\pi^0$  fragmentation functions in NLO have been developed recently [9]. This has not been done for charged particles yet, in which we are mainly interested here. The existing information on fragmentation functions of charged particles is based on fits to data from  $e^+e^-$  annihilation and deep-inelastic lepton-nucleon scattering in connection with LO evolution [10,11]. These LO fragmentation functions have been tested in inclusive charged-particle production in  $p\bar{p}$  scattering in a previous communication [12], henceforth referred to as **I**. Reasonably good agreement with existing data from the UA2 and CDF Collaborations has been found. Since the center-of-mass (CM) energies in these experiments,  $\sqrt{s} = (540-1800)$  GeV, are even higher than the HERA CM energy,  $\sqrt{s} = 298$  GeV, we feel confident that these LO functions give a reasonable account of the fragmentation of quarks and gluons into charged hadrons.

The NLO corrections to the parton-level cross sections appropriate for inclusive single-particle production have been worked out by Aversa et al. [13]. They provide the basis of the NLO corrections to charged-particle and neutral-pion production presented here.

In this paper we shall predict cross sections of single-charged hadron and single- $\pi^0$  production in low- $Q^2$   $ep$  reactions at the HERA energy. This work is an extension of **I**, where inclusive hadron production in  $p\bar{p}$  collisions was studied. The formalism used here is quite

similar. One has to adjust the initial state and take care of the fact that the incoming electron produces a spectrum of photons, which is usually described in the Weizsäcker-Williams approximation (WWA) [14]. Compared to  $p\bar{p}$  collisions, we expect in  $\gamma p$  processes a different behaviour of the cross section due to the presence of the point-like component in the photon structure function.

Experimental data of charged-particle and  $\pi^0$  production at relatively low CM energies come from fixed-target experiments at CERN [15]. In these experiments the resolved-photon component could not be separated from the direct one. Resolved photoproduction cross sections for single hadrons have already been measured at HERA [1]. A better statistic is now being accumulated and a wider range of  $p_T$  is under study. These data will probe the QCD-improved parton model in an energy regime that lies between  $\sqrt{s} = 200$  GeV, the  $p\bar{p}$  CM energy of UA1, and  $\sqrt{s} = 540$  or 630 GeV as used by UA1, UA2, and CDF.

The outline of this paper is as follows. In Sect. 2, we give a brief introduction to the theoretical input and the structure functions used for the calculation. Numerical results are presented in Sect. 3, where we compare with the first data from the H1 Collaboration. Section 4 is reserved for a discussion of the results and some outlook to future work.

## 2 Theoretical ingredients and structure functions

When we speak of photoproduction with almost real photons we have in mind the class of  $ep$  processes where the electron is a source of nearly massless, collinear photons, which collide with the opposing proton beam. The energy spectrum for the resulting photons is calculated in the WWA. In this approximation the longitudinal- and transverse-momentum components of the photon distribution decouple. The transverse momentum is integrated out with an angular cut of  $\theta_{\max} = 5^\circ$ . Then the distribution in the longitudinal-momentum fraction,  $x$ , of the outgoing photon has in the leading-logarithm approximation the following form [14]:

$$f_{\gamma/e}(x) = \frac{\alpha}{\pi} \frac{1 + (1-x)^2}{x} \ln \frac{E_e \theta_{\max}}{m_e}, \quad (2.1)$$

where  $E_e$  is the electron energy,  $m_e$  is the electron mass, and  $x E_e$  is the photon momentum. Equation (2.1) determines the photon luminosity used in our calculation. When comparing with experimental data, the

actual electron acceptance must be incorporated. This will affect our results only through a normalization factor of (2.1). Then in the WWA the inclusive single-particle cross section is related to the corresponding photoproduction cross section in the following way:

$$E_h \frac{d^3\sigma(ep \rightarrow hX)}{d^3p_h} = \int_{x_{\min}}^1 dx f_{\gamma/e}(x) E_h \frac{d^3\sigma(\gamma p \rightarrow hX)}{d^3p_h} \quad (2.2)$$

On the right-hand side of (2.2),  $x E_e$  is substituted for the photon momentum and  $x_{\min}$  is expressed in terms of transverse momentum,  $p_T$ , and CM rapidity,  $y_{\text{CM}}$ , of the produced hadron as

$$x_{\min} = \frac{p_T e^{y_{\text{CM}}}}{\sqrt{s} - p_T e^{-y_{\text{CM}}}}. \quad (2.3)$$

The rapidity measured in the laboratory frame,  $y_{\text{lab}}$ , is related to  $y_{\text{CM}}$  by

$$y_{\text{lab}} = y_{\text{CM}} - \frac{1}{2} \ln \frac{E_p}{E_e}, \quad (2.4)$$

where the energies of the electron and the proton,  $E_e$  and  $E_p$ , are in the laboratory frame. According to current HERA conditions,  $E_e = 27$  GeV and  $E_p = 820$  GeV, so that  $y_{\text{lab}} = y_{\text{CM}} - 1.71$ .

In the QCD-improved parton model the single-particle photoproduction cross section on the right-hand side of (2.2) is expressed in LO as a convolution of the LO parton-parton scattering cross section with the scale-dependent structure and fragmentation functions. We fix the momenta of photon, proton and outgoing hadron ( $h$ ) by

$$\gamma(p_\gamma) + p(p_p) \rightarrow h(p_h) + X. \quad (2.5)$$

In this way, the notation is similar to the one used in I. Mutatis mutandis, the LO cross section is given by

$$E_h \frac{d^3\sigma^0}{d^3p_h} = \sum_{i,j,l} \int dx_\gamma \int dx_p \int \frac{dx_h}{x_h^2} F_i^{\gamma}(x_\gamma, M^2) \times F_j^p(x_p, M^2) D_l^h(x_h, M_f^2) k_l^0 \frac{d^3\sigma_{k_i k_j \rightarrow k_l}^0}{d^3k_l}, \quad (2.6)$$

where  $k_i = x_\gamma p_\gamma$ ,  $k_j = x_p p_p$ , and  $k_h = p_h/x_h$  are the parton momenta. The indices  $i, j, l$  run over gluons and  $N_F$  flavours of quarks. We assume  $N_F = 4$  throughout our calculation and include the charm-quark threshold as implemented in the photon structure function parametrizations used.  $F_j^p(x_p, M^2)$  is the proton structure function appropriate for parton  $j$  and  $D_l^h(x_h, M_f^2)$  is the fragmentation function of parton  $l$  into hadron  $h$ .  $M$  is the factorization scale of the photon and proton structure functions, which we assume to be equal,

$M_f$  is the scale of the fragmentation function. Finally,  $d^3\sigma_{k_i k_j \rightarrow k_l}^0$  describes the process  $i + j \rightarrow l + X$  in  $\mathcal{O}(\alpha_s^2(\mu^2))$ .

The calculation of the NLO inclusive cross section is described in **I**. The relevant formulae are used with the replacement  $F_i^{h_1}(x_1, M^2) \rightarrow F_i^\gamma(x_\gamma, M^2)$  and  $F_j^{h_2}(x_2, M^2) \rightarrow F_j^p(x_p, M^2)$ . For the full calculation we need the structure functions of the photon and the proton and the fragmentation functions in NLO. As already mentioned in the introduction, fragmentation functions exist only in LO, except for the recently constructed  $\pi^0$  set [9]. We shall use the same fragmentation functions as in **I**, namely those of Baier et al. [10] and Anselmino et al. [11] with the constraints specified in **I**. Since these fragmentation functions correspond approximately to the  $\overline{\text{MS}}$  factorization, we have also selected the  $\overline{\text{MS}}$  scheme for the proton and photon structure functions.

The proton structure function parametrizations are again taken from the package by Charchula [17]. For most part of our analysis we use the Morfin-Tung (MT) set B1 in the  $\overline{\text{MS}}$  version.

For the NLO photon structure functions we have three sets at our disposal [6,7,8]. All three have been tested against the available data on the photon structure function  $\mathcal{F}_2^\gamma(x, Q^2)$ . Unfortunately, this leaves still appreciable freedom, in particular with respect to the gluon content of the photon. For our main results we use the sets by Glück, Reya, and Vogt (GRV) [6] with  $N_F = 4$ . In their analysis the  $Q^2$  evolution starts with a valence-like input at a rather small scale,  $Q_0^2$ , which is  $Q_0^2 = 0.25 \text{ GeV}^2$  in the LO fit and  $Q_0^2 = 0.3 \text{ GeV}^2$  in the NLO fit, respectively. Their NLO set refers to the so-called deep-inelastic  $\gamma$  scattering (DIS $\gamma$ ) scheme. For consistency in our analysis, we convert the GRV DIS $\gamma$  set into the more familiar  $\overline{\text{MS}}$  scheme. For comparative studies at the LO level of the hard scattering we use also the LO set by GRV. Besides, we make use also of the LO set by Drees and Grassie (DG) [18] and the NLO set by Aurenche et al. (ACFGP) [8] to investigate the sensitivity of the cross section to different choices. The boundary conditions used by ACFGP are similar to those of GRV and the evolution is started at  $Q_0^2 = 0.25 \text{ GeV}^2$ . The gluon content of the photon is particularly low in the ACFGP set. The charm distribution is totally described by the lowest-order expression, which has its starting point at  $Q_0^2 = 2 \text{ GeV}^2$ . Gordon and Storrow (GS) [7], on the other hand, start the  $Q^2$  evolution at  $Q_0^2 = 5.3 \text{ GeV}^2$ , which is considerably larger than the values of GRV and ACFGP.

In the next section we shall present the results in two steps. In the first step, we assume that  $D_l^h(x_h, M_f^2)$

$= \delta(1 - x_h)$  for all hadrons  $h$  and partons  $l$ . In this way, we study the cross sections for the production of single partons. In LO they are identical to the single-jet production cross sections. In NLO they depend on the factorization scale  $M_f^2$  and cannot be compared to jet production cross sections, since the recombination algorithm for defining jets is not built in. However, the cross section with  $\delta$ -function fragmentation are simpler to calculate and reveal several features that are also relevant for the complete single-particle cross sections considered in the second step.

## 3 Numerical results

### 3.1 Single-parton inclusive cross sections

In this sub-section we approximate all fragmentation functions by  $\delta$  functions. This leads to single-parton inclusive cross sections. For a first orientation, we disentangle the various parton-parton channels that contribute in LO to the hard-scattering cross sections ordering them according to their initial state, viz.

- 1)  $gg \rightarrow gg, q\bar{q}$ ,
- 2)  $gq \rightarrow gq, qg$ ,
- 3)  $qq \rightarrow gq, qg$ ,
- 4)  $q\bar{q} \rightarrow gg, q\bar{q}, \bar{q}q, q'q'$ ,  
 $qq \rightarrow qq$ ,  
 $qq' \rightarrow qq', q'q$ ,

where  $q$  and  $q'$  denote different quark flavours. The first parton originates from the photon, the second from the proton. These four classes of channels are also compared with direct photoproduction in LO, which proceeds through  $\gamma g \rightarrow q\bar{q}$  and  $\gamma q \rightarrow gq, qg$ . The comparison is done for  $d^2\sigma/dy dp_T$  at  $\sqrt{s} = 298 \text{ GeV}$  (this corresponds to 27 GeV electrons colliding with 820 GeV protons according to present HERA conditions) and  $y_{\text{lab}} = -2$  (with  $y_{\text{lab}} > 0$  in the direction of the electron momentum). For this calculation we use the LO set SL of the MT proton structure functions and the LO set of the GRV photon structure functions. We also fix the two scales  $\mu$  and  $M$  to be  $\mu = M = p_T$ .

In Fig. 1 we show the  $p_T$  dependence of the channels 1)-4) contributing to the resolved  $\gamma p$  cross section and the  $p_T$  dependence of the direct process. We observe that at small  $p_T$  channels 1), 2), and 3) dominate

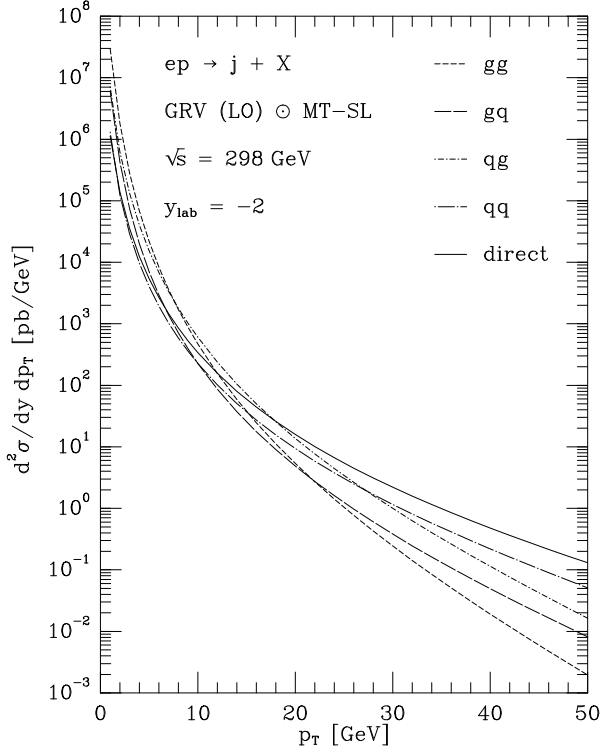


**Fig. 1.** Transverse-momentum distributions of the various channels for resolved photoproduction and of direct photoproduction in LO at  $\sqrt{s} = 298$  GeV and  $y_{\text{lab}} = -2$  evaluated with the LO sets by GRV and MT-SL. The resolved-photon channels are grouped according to their parton-parton initial state; the first parton originates from the photon and the second from the proton

by one order of magnitude over class 4) and the direct mechanism, whereas at larger  $p_T$  ( $p_T \gtrsim 28$  GeV) class 4), in particular the channels involving quarks only, contribute significantly. It is exactly in this  $p_T$  range, more precisely for  $p_T > 35$  GeV, that the direct process exceeds the sum of the resolved processes. The pattern observed for the various resolved photoproduction channels is similar to the situation encountered in **I** in the case of  $p\bar{p}$  collisions: the gluon components of the photon and proton structure functions influence strongly the cross section at smaller  $p_T$ , whereas the pure quark channels dominate at larger  $p_T$ .

In Fig. 2, the rapidity distributions of the above channels are displayed for fixed  $p_T = 5$  GeV. For  $y_{\text{lab}} < 0$ , i.e., in the proton direction, classes 1) and 3) dominate and the direct mechanism comes in only in the extreme forward direction, at  $y_{\text{lab}} \approx 1$ . Of course, the relative size of the various classes in Figs. 1,2 may change when realistic fragmentation functions are taken into account.

Next we study how our results are changed when different sets of proton structure functions are em-

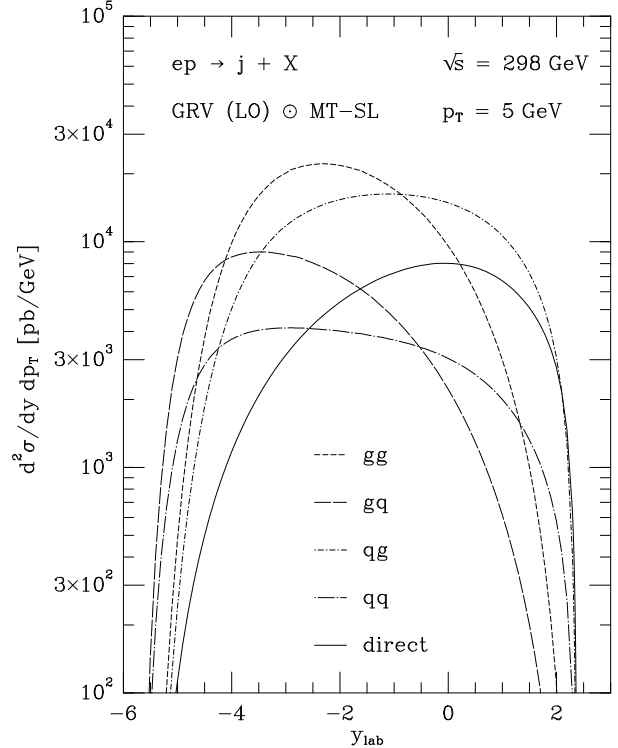


**Fig. 2.** Rapidity distributions of the various channels for resolved photoproduction and of direct photoproduction in LO at  $\sqrt{s} = 298$  GeV and  $p_T = 5$  GeV evaluated with the LO sets by GRV and MT; see caption of Fig. 1

ployed. Toward this end, we calculate  $d^2\sigma/dy dp_T$  in the Born approximation at  $\sqrt{s} = 298$  GeV and  $y_{\text{lab}} = -2$  as a function of  $p_T$  using in turn the proton structure function sets MT-B1 (DIS), MT-B1 ( $\overline{\text{MS}}$ ) [3] and MRSn-D0 ( $\overline{\text{MS}}$ ), MRSn-D- ( $\overline{\text{MS}}$ ) [5], which are all of NLO. For the photon structure functions we choose the LO set by GRV [6] and for the QCD coupling  $\alpha_s$  we use the usual one-loop formula adopting the value of  $\Lambda$  from the respective proton structure functions. In Fig. 3, we show the cross sections normalized with respect to the calculation with the MT-SL set. We remark that only the MT-SL set should be combined with the LO hard-scattering cross sections because it is a genuine LO fit; all the others correspond to NLO analyses of present data.

We observe that the variation caused by replacing the LO set by the various NLO sets does not exceed 30% for  $p_T \gtrsim 2$  GeV. A similar result was found in **I** for  $p\bar{p}$  processes. We observe that the ratio of the two cross sections is always larger than one. From what was said above, it follows that the comparison of the NLO sets with the LO set is not particularly meaningful. However, it is instructive to compare the results obtained with different NLO sets of proton structure functions parametrizations. The corresponding

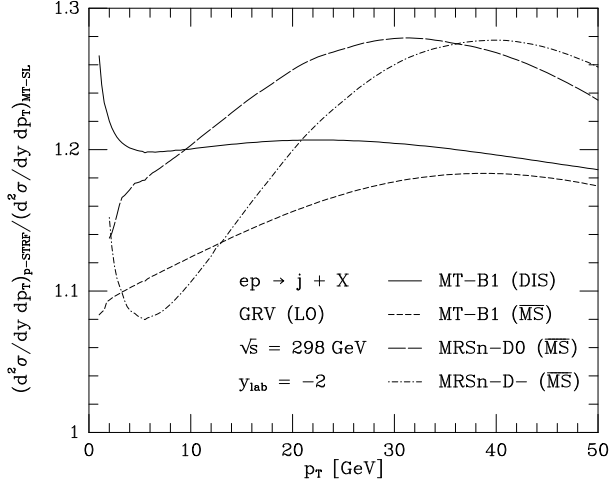


**Fig. 3.** Influence of typical NLO proton structure functions on the LO calculation of  $d^2\sigma/dy dp_T$  for resolved photoproduction at  $\sqrt{s} = 298$  GeV and  $y_{\text{lab}} = -2$ . The curves are normalized to the LO calculation with the MT-SL set. In both numerator and denominator the GRV LO photon structure functions are used

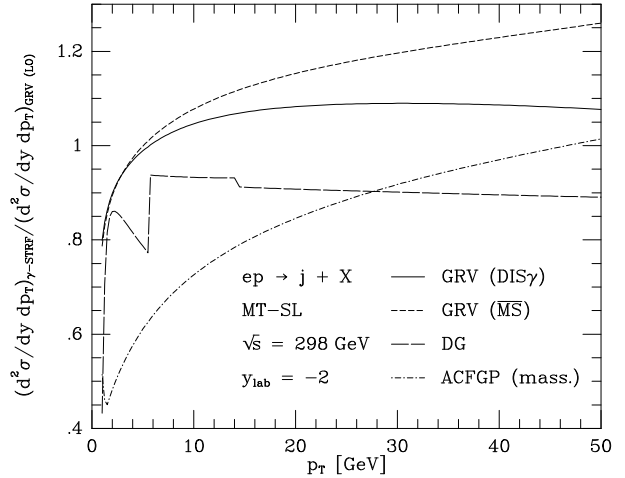


**Fig. 4.** Influence of typical photon structure functions on the LO calculation of  $d^2\sigma/dy dp_T$  for resolved photoproduction at  $\sqrt{s} = 298$  GeV and  $y_{\text{lab}} = -2$ . The curves are normalized to the LO calculation with the GRV LO set. In both numerator and denominator the MT-SL proton structure functions are used

cross sections differ at most by 20%. The DIS and  $\overline{\text{MS}}$  versions of MT-B1 differ by only 10% relatively to each other. We consider this as an upper bound on the scheme dependence, since the partial compensation that is expected to take place at NLO, due to scheme-dependent terms, is not in effect here. The MRSn-D0 and MRSn-D- sets fit also recent NMC [19] and CCFR [20] data, which extend to smaller values of  $x$  than previously tested. The D0 and D- sets, available in the  $\overline{\text{MS}}$  version, give cross sections with quite different behaviours at low  $p_T$ . At large  $p_T$  they give similar results and differ from the cross section obtained making use of the MT-B1 ( $\overline{\text{MS}}$ ) set by (10–15)%. When comparing with the pattern observed for  $p\bar{p}$  reactions (see Fig. 2 in I), we must keep in mind that there the structure functions of both proton and antiproton are changed, whereas here the photon structure function is left unchanged.

To study the influence of different photon structure functions, we calculate  $d^2\sigma/dy dp_T$  again in the Born approximation at  $\sqrt{s} = 298$  GeV and  $y_{\text{lab}} = -2$  as a function of  $p_T$  using in turn the NLO sets GRV (DIS $\gamma$ ), GRV ( $\overline{\text{MS}}$ ) [6], ACFGP (massive) [8] and GS [7] and the LO parametrizations GRV [6], DG [18] and GS [7]. In all cases the MT-SL proton structure function parametrization is used. The results are shown in Fig. 4. Except for low  $p_T$ , the DG set gives cross sections which are 10% smaller than those for GRV (LO). The two steps in the DG curve are due to the fact that the DG parametrization is discontinuous at the charm and bottom thresholds, at  $p_T \approx 5$  GeV and

$p_T \approx 14$  GeV, respectively. The GRV structure functions are smooth at these thresholds. The GRV (DIS $\gamma$ ) set gives results very close to the GRV (LO) results. This set involves a particular subtraction in the point-like part of the photon structure function, which is compensated by a change of the direct photoproduction cross section. Since the latter is beyond the scope of this work, we shall not employ the GRV (DIS $\gamma$ ) set in the following. We observe that the DIS $\gamma$  and  $\overline{\text{MS}}$  versions of the GRV parametrization differ appreciably only at larger  $p_T$ , where direct photoproduction comes into play; at small  $p_T$  ( $p_T \lesssim 25$  GeV) their difference is below 10%. The cross section for the ACFGP choice of structure functions, which is also based on the  $\overline{\text{MS}}$  scheme, is very different, especially in the lower- $p_T$  range, where it is up to 50% smaller than the GRV results. This can be traced to the much weaker gluon component in the ACFGP set. At large  $p_T$ , where the influence of the gluon component diminishes, the ratio approaches the value 1 again. The results obtained for the LO and NLO GS photon structure function are not included in Fig. 4. The LO soft-gluon option yields values for the ratio between 1 and 1.2 for  $p_T \lesssim 16$  GeV. In the upper range of the  $p_T$  values considered in Fig. 4 the ratio comes down to 0.9. The NLO set, which is based on the  $\overline{\text{MS}}$  scheme, gives results in the ballpark of those obtained with the DG and ACFGP sets; for  $p_T \lesssim 20$  GeV the GS ( $\overline{\text{MS}}$ ) values are somewhat smaller than the DG values, for  $p_T \gtrsim 30$  GeV they are in line with the ACFGP values.

To investigate the influence of the higher-order terms of the hard-scattering cross sections, we restrict ourselves to pure photoproduction, replacing the right-hand side of (2.1) by  $\delta(1-x)$ . We calculate  $d^2\sigma(\gamma p \rightarrow hX)/dy dp_T$  at  $\sqrt{s} = 256$  GeV (corresponding to typical 20 GeV photons colliding with 820 GeV protons) and  $y_{\text{lab}} = -2$  as a function of  $p_T$  with and without the higher order terms and plot the ratio in Fig. 5. This ratio should change only little when the photon spectrum (2.1) is taken into account. A realistic analysis including the WWA and also fragmentation will be reported in the next sub-section. At this point, we wish to separate the effect of the higher-order terms. To that end, we use the same structure functions, namely the  $\overline{\text{MS}}$  versions of GRV and MT-B1, and the two-loop expression for  $\alpha_s$  in both numerator and denominator. The renormalization scale of  $\alpha_s$  is adjusted according to the proton structure functions, i.e.,  $\Lambda = 194$  MeV, which is very close to the value  $\Lambda = 200$  GeV ( $N_F = 4$ ) implemented in the GRV set. We perform the computation for the three choices  $\mu = M = M_f = p_T/2$ ,  $p_T$ , and  $2p_T$ . From Fig. 5 we see that the ratio is practically independent of  $p_T$  for  $p_T \gtrsim 10$  GeV. For smaller  $p_T$  it increases with decreasing  $p_T$  at a rate that is largest for the smallest scale. Its value ranges between 1.5 and 2.5, which demonstrates the importance of the NLO corrections to the parton-level cross sections. These results are very similar to the ones reported in **I** for  $p\bar{p}$  reactions at  $\sqrt{s} = 630$  GeV. Note that, in contrast to Figs. 3 and 4, the same structure functions are used in both numerator and denominator, so that variations due to changes of scheme or parametrization largely cancel out. We observe a strong scale dependence, which is mainly due to the denominator, as will become apparent below.

At this point, a few comments on spurious higher-order effects are in order. In Fig. 5, we used NLO structure functions also in connection with the NLO corrections to the hard-scattering cross sections. Strictly speaking, such a procedure introduces certain contributions beyond next-to-leading order in the case of GRV. For the choice  $\mu = M = M_f = p_T$  we have explicitly checked the influence of the modifications necessary to eliminate these spurious higher-order terms. At small  $p_T$  ( $p_T \lesssim 5$  GeV), the ratio is increased by some 10%, but already at  $p_T \gtrsim 7$  GeV the increase becomes insignificant, until it vanishes at  $p_T \sim 12$  GeV. Then the ratio is reduced by an amount which reaches at most 5% at the upper end of the  $p_T$ -range shown in Fig. 5. Similar results are obtained for single-hadron production: the only effect of the realistic fragmentation functions is to reduce the values of  $p_T$  at which the features previously described take place. Since at present there is still appreciable freedom concerning the details of

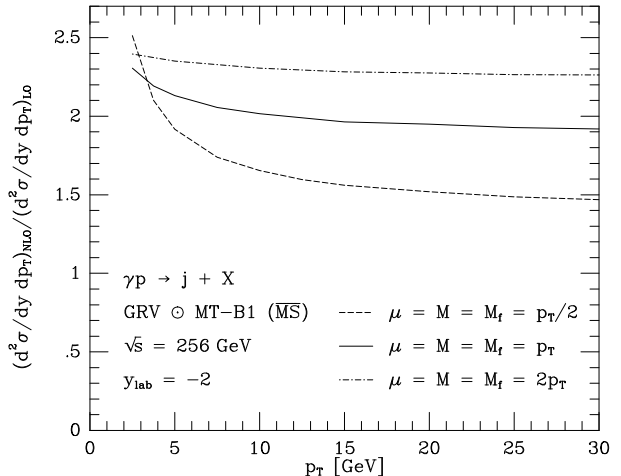


**Fig. 5.** NLO calculation in the  $\overline{\text{MS}}$  scheme of  $d^2\sigma/dy dp_T$  for  $\gamma p \rightarrow j + X$  at  $\sqrt{s} = 256$  GeV and  $y_{\text{lab}} = -2$  normalized to the corresponding calculation with the NLO terms in the hard-scattering cross section omitted. In both numerator and denominator the  $\overline{\text{MS}}$  sets of the GRV and MT-B1 structure functions are used. The scales  $\mu$ ,  $M$ , and  $M_f$  are identified and set equal to  $p_T/2$ ,  $p_T$ , and  $2p_T$

the photon structure functions, we do not consider it necessary to worry about this complication, leaving it for a future, more refined analysis.

The scale dependence of numerator and denominator of the ratio plotted in Fig. 5 is explicitly investigated in Figs. 6a,b for  $p_T$  fixed at 10 and 20 GeV, respectively. The three scales  $\mu$ ,  $M$ , and  $M_f$  are set equal to  $\xi p_T$  and  $\xi$  is varied between 0.2 and 5.0. Again, we choose the  $\overline{\text{MS}}$  sets by GRV and MT,  $\sqrt{s} = 256$  GeV, and  $y_{\text{lab}} = -2$ . The LO cross section (dashed line) depends more strongly on the scale  $\xi$  than the NLO result (solid line). The more rapid decrease of the LO cross section for increasing  $\xi$  explains the increase of the ratio plotted in Fig. 5. The NLO cross section is particularly insensitive to  $\xi$  for  $\xi > 0.5$ . This holds true independently of  $p_T$ , although the absolute cross section strongly varies with  $p_T$ . The scale variation of the NLO cross section is well bounded in contrast to the LO cross section, which decreases monotonically with increasing  $\xi$ . At this point, one should keep in mind that the  $M_f$  dependence in the NLO hard-scattering cross section is not compensated as long as  $\delta$ -function-type fragmentation is assumed. If we do not vary  $M_f$ , which would be more appropriate in this case, we obtain the dot-dashed curves in Figs. 6a,b. This shows less  $\xi$  dependence than the LO curves but more than the NLO curves with variable  $M_f$ . It seems that the factorization scale dependence in the NLO hard-scattering cross section is mostly cancelled between initial and final state. The pattern observed in Figs. 6a,b is very

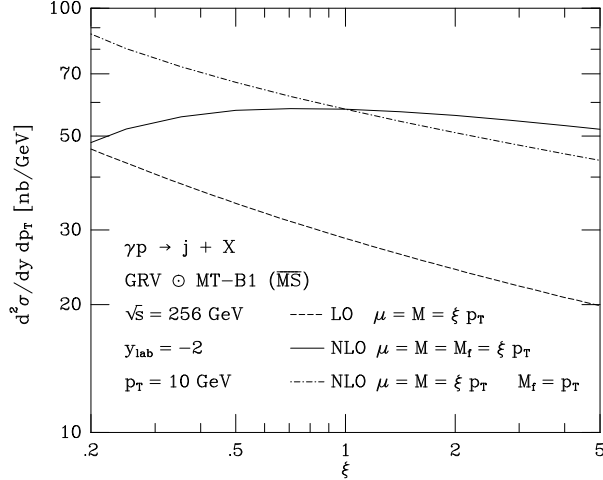


**Fig. 6a.** Scale dependence of  $d^2\sigma/dy dp_T$  for  $\gamma p \rightarrow j + X$  at  $\sqrt{s} = 256$  GeV,  $y_{\text{lab}} = -2$ , and  $p_T = 10$  GeV. The solid and dot-dashed lines represent the NLO results in the  $\overline{\text{MS}}$  scheme with variable and fixed  $M_f$ , respectively. The  $\overline{\text{MS}}$  sets of the GRV and MT-B1 structure functions are used. The dashed lines correspond to the calculation with the NLO terms of the hard-scattering cross sections omitted

similar to our findings regarding  $p\bar{p}$  collisions in **I**.

### 3.2 Single-hadron inclusive cross sections

In this sub-section we shall present our results for the inclusive production of single charged hadrons and neutral pions. For the calculation of these cross sections we used the same fragmentation functions as in Sect. 2. We choose the MT-B1 and GRV structure functions, both in the  $\overline{\text{MS}}$  scheme, except in Fig. 7, where we

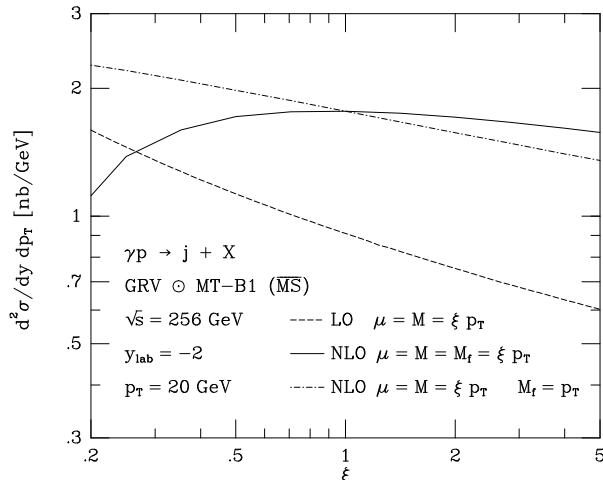


**Fig. 6b.** Same as in Fig. 6a but at  $p_T = 20$  GeV.

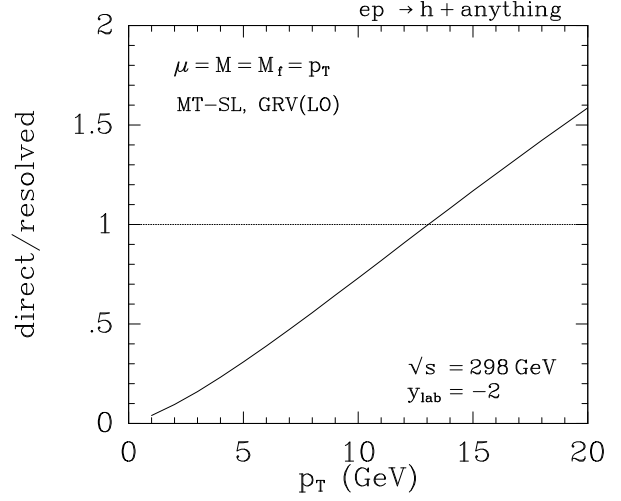


**Fig. 7.** Ratio of direct over resolved contribution to the cross section for production of charged hadrons

take the MT-SL and GRV (LO) structure functions. As in the previous sub-section, the parameter  $\Lambda$  in the coupling constant  $\alpha_s$  is set equal to the value required by the proton structure function parametrizations, i.e. 194 MeV for NLO evaluations and 144 MeV for the LO ones.

First we consider the ratio of direct over resolved production of charged hadrons  $h \equiv (h^+ + h^-)/2$  in order to see where they are equal in magnitude. We restrict ourselves to the LO calculation and we set  $\sqrt{s} = 298$  GeV,  $y_{\text{lab}} = -2$ , and  $\mu = M = M_f = p_T$ . As in the previous sections,  $M$  indicates both, the factorization scales for the photon and the proton structure functions. The result is shown in Fig. 7. The crossing point, above which the direct production of single hadrons exceeds the resolved one, is at  $p_T \sim 13$  GeV. This value is considerably lower than the crossing point obtained in the case of LO jet-production cross section. We do not expect the position of these points to change drastically when NLO corrections are included. Fig. 7 shows clearly that for  $p_T > 5$  GeV the direct production of single charged hadrons is not negligible anymore and our results can only apply to data with a visible photon remnant jet.

In Fig. 8 we show  $d^2\sigma/dy dp_T$  for inclusive single-charged hadron production as a function of  $p_T$  for  $\sqrt{s} = 298$  GeV,  $y_{\text{lab}} = -2$ , and  $\mu = M = M_f = p_T$ . The upper curve is the NLO result and the lower curve the LO cross section with the same structure functions, MT-B1 and GRV in  $\overline{\text{MS}}$ , and  $\alpha_s(\mu^2)$ . K factors ranging between 2.5 and 1.6 are obtained in the  $p_T$  range considered here. They are smaller at high  $p_T$  than the factors observed in the case of  $\delta$ -function fragmentation (see Fig. 5), for the same choice of scales, but



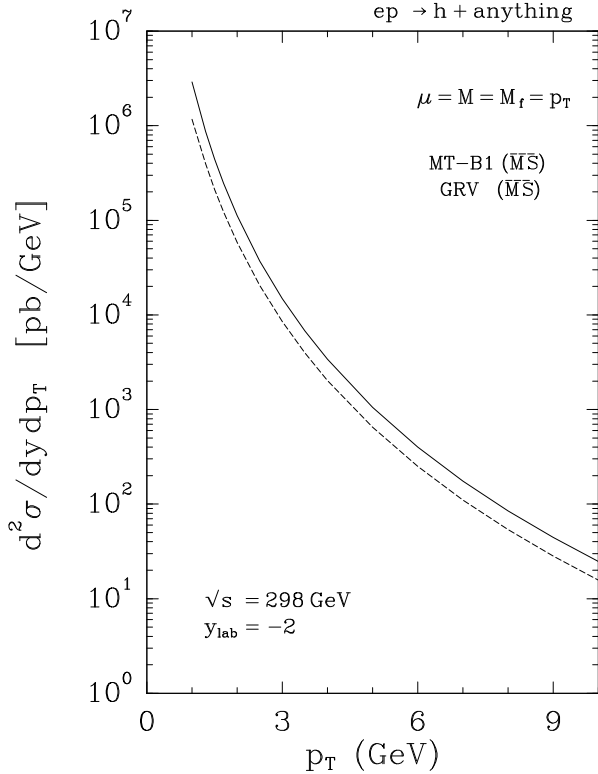


**Fig. 8.** Inclusive charged-hadron production cross section for  $\sqrt{s} = 298$  GeV and  $y_{\text{lab}} = -2$ . The solid line correspond to the NLO prediction while the dashed line is the LO result obtained with structure functions and  $\alpha_s$  kept at the NLO level

bigger at high  $p_T$ . Moreover, the inclusion of realistic fragmentation functions for the produced hadrons induces a decrease of the cross section, for increasing  $p_T$ , faster than the one observed in Fig. 1.

Qualitatively similar results, shown in Fig. 9, are obtained in the case of single- $\pi^0$  production. However, the values of the cross sections are here lower than the ones obtained in the case of charged-hadron production, for the same choice of scales. It should be reminded at this point that the results presented in **I** for single- $\pi^0$  production in  $p\bar{p}$  collisions could fit the existing data only for relatively high scales. Similar conclusions were reached in [9] when the  $\pi^0$ -fragmentation functions [11] were used.

In connection with the results in Figs. 8 and 9, it is of interest to know the influence on the cross section of the gluon originating from the photon. According to the results shown in Fig. 1, we expect this gluon contribution to be more important at small  $p_T$ . In Fig. 10 we plot the  $p_T$  dependence of the ratio

$$R_{g/\gamma} \equiv \frac{d^2\sigma/dy dp_T - d^2\sigma/dy dp_T|_{(\text{no } g/\gamma)}}{d^2\sigma/dy dp_T}, \quad (2.7)$$

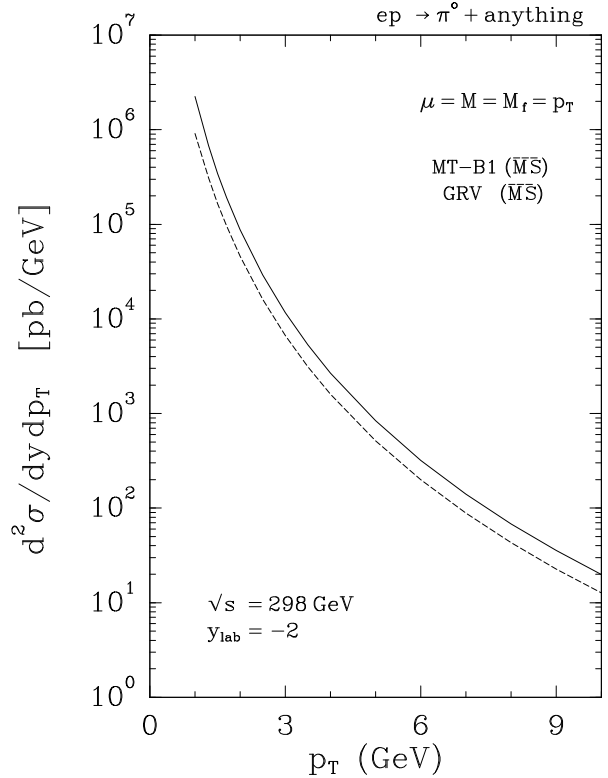


**Fig. 9.** Same as in Fig. 8 for single- $\pi^0$  production

where the label (no  $g/\gamma$ ) indicates that the gluon component in the photon has been put to zero.  $R_{g/\gamma}$  varies from 60% at  $p_T = 2$  GeV to 30% at  $p_T = 10$  GeV. This result is essentially independent of whether NLO corrections are included or not.

The importance of the quark component of the photon for increasing  $p_T$  should become evident when we compare single-charged hadron production in  $ep$  and  $p\bar{p}$  collisions at the same  $\sqrt{s}$ . Since, at large  $p_T$ , the point-like part of the photon-quark component is much stronger than the proton-quark distribution, we expect the  $p\bar{p}$  cross section to fall off more rapidly than the  $ep$  cross section, for increasing  $p_T$ . This is indeed the case, as can be seen in Fig. 11 where we compare  $ep \rightarrow hX$  via resolved photons with  $p\bar{p} \rightarrow hX$  at  $\sqrt{s} = 298$  GeV and a CM rapidity at which both cross sections are maximal,  $y_{\text{CM}} = -0.3$ . The two curves in Fig. 11 are NLO (upper curves) and LO (lower curves) predictions, respectively. The values of the  $ep$  cross section have been multiplied by the factor 3000 which makes  $ep$  and  $p\bar{p}$  results coincide up to  $p_T \sim 4$  GeV. Already at  $p_T = 10$  GeV, though, the two sets of curves deviate visibly from each other and at the upper end of the  $p_T$ -range shown in Fig. 11 the  $p\bar{p}$  cross section falls short of the  $ep$  one by at least a factor two. Of course, in order to verify this effect experimentally, we need  $p\bar{p}$  and  $ep$  data at the same  $\sqrt{s}$  and the isolation of the

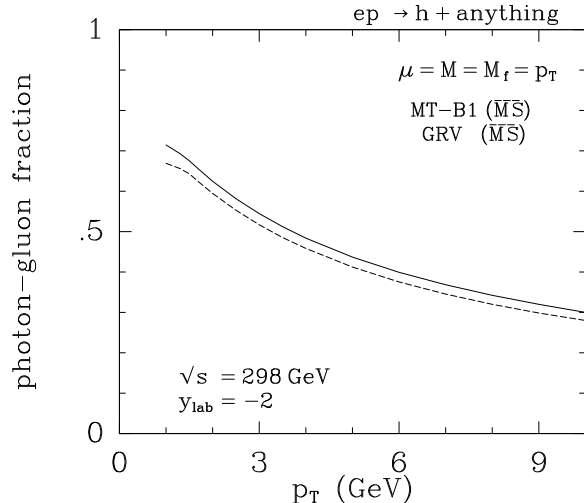


**Fig. 10.** Fraction  $R_{g/\gamma}$  of the charged-hadron production cross section at  $\sqrt{s} = 298$  GeV and  $y_{\text{lab}} = -2$  due to the gluon originating from the photon. The solid line indicates the NLO result and the dashed line the LO one with structure functions and  $\alpha_s$  at the NLO level

resolved production in the  $ep$  process. With direct  $ep$  production included, the effect should be even stronger.

Another issue to be considered before proceeding further is whether the inclusion of a fifth flavour introduces any appreciable deviation from the results presented so far. We have verified that, in spite of the non-negligible contribution of the bottom-quark to the photon structure function, the increase in the cross sections is at most 2%, for the highest  $p_T$  values here considered, when we assume  $N_f = 5$ .

Finally, in Fig. 12 we compare our predictions from Fig. 8 with recent data obtained by the H1 Collaboration at HERA [1]. These data extend only up to  $p_T^2 = 12$  GeV<sup>2</sup> and have quite large experimental uncertainties for the largest values of  $p_T^2$ . Since the absolute normalization of these data points is not known, we have adjusted them with an overall factor so as to have satisfactory agreement with the theoretical NLO results at  $p_T^2 \sim 1.4$ – $1.7$  GeV<sup>2</sup>. We see that the  $p_T^2$  shape of the theoretical results is consistent with the data. Of course, for firmer conclusions, more accurate data which extend to higher values of  $p_T^2$  are needed.

To obtain more information on the scale dependence of the inclusive cross section, we have calculated it as a function of the scale factor  $\xi$  defined in the previous sub-section for  $p_T = 3, 5$  and  $10$  GeV and  $\sqrt{s} = 298$  GeV,  $y_{\text{lab}} = -2$ . The results are shown in Fig. 13, where we compare the NLO predictions evaluated with MT-B1 and GRV in  $\overline{\text{MS}}$  and two-loop  $\alpha_s$  (solid lines) with the LO predictions evaluated with

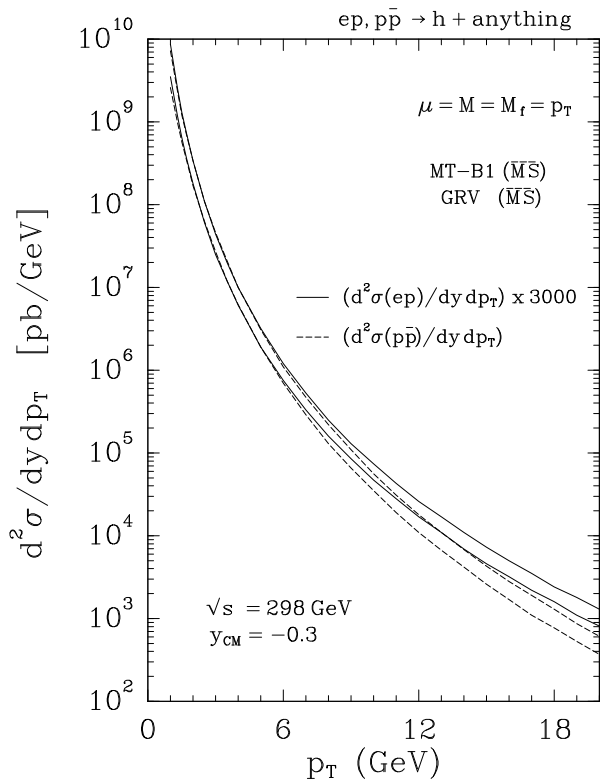


**Fig. 11.** Comparison of the cross sections of charged-hadron production in  $p\bar{p}$  collisions and via resolved photons in  $ep$  collisions at HERA energy and the same CM energy and rapidity,  $\sqrt{s} = 298$  GeV and  $y_{\text{CM}} = -0.3$ . The upper curves indicate the full NLO results, while the lower ones give the LO results obtained with structure function and  $\alpha_s$  at the NLO level

MT-SL and GRV (LO) and one-loop  $\alpha_s$  (dotted lines). To show the effect of the  $\mathcal{O}(\alpha_s^3)$  terms in the hard-scattering cross section, we also plot the results obtained for the LO predictions when structure function and  $\alpha_s$  are kept at the NLO level.

We see quite clearly that the NLO cross section has less scale dependence than the two LO ones. Except than for the case  $p_T = 3$  GeV, the NLO cross section develops a plateau for  $\xi = 0.6$ . The turn-over for small  $\xi$  at  $p_T = 10$  GeV is presumably an artifact due to the use of LO fragmentation functions. Both LO curves show a monotonic dependence on  $\xi$ , which for  $\xi > 1$  is steeper than the dependence of the NLO cross section. We also observe that the LO cross sections (dotted curves) equal the NLO ones for  $\xi$  between 0.6 and 0.9, whereas at larger values of  $\xi$  the two sets of curves are quite well separated. These latter feature has also been observed in **I** for single-charged hadron production in  $p\bar{p}$  collisions.

A comparison of Fig. 13 for  $p_T = 10$  GeV with

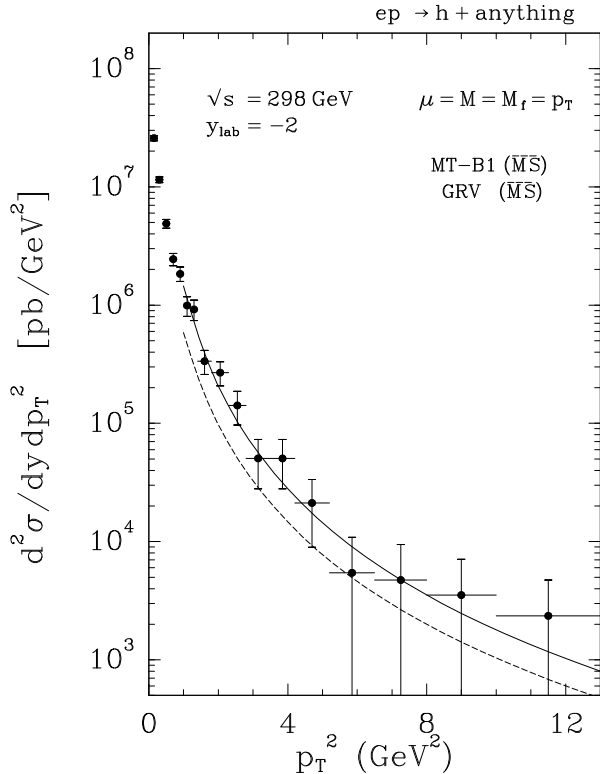


**Fig. 12.** Comparison between the theoretical predictions for the resolved-photon contribution to  $ep \rightarrow hX$  and the experimental data obtained by the H1 Collaboration at HERA [1]. The data are normalized globally in such a way that they match with the NLO prediction at  $p_T^2 \sim 1.4\text{--}1.7 \text{ GeV}^2$ . The solid line indicates the NLO prediction and the dashed line the LO one obtained with structure functions and  $\alpha_s$  at the NLO level

Fig. 6a, where the scale dependence has been investigated in the case of  $\delta$ -function fragmentation and real photoproduction at  $\sqrt{s} = 256 \text{ GeV}$ , yields the following observations. Apart from the absolute size, the LO results exhibit roughly the same qualitative features, which is attributed to a rather weak scale dependence of the LO fragmentation functions. The situation changes when NLO corrections are included. The drop-off at small  $\xi$  is stronger in Fig. 13 than in Fig. 6a. Finally, higher scales are needed to obtain equal values of LO and NLO results when realistic fragmentation functions are included.

So far we have concentrated on the discussion of  $p_T$  distributions for fixed  $y_{\text{lab}} = -2$ , where cross sections are maximal. In Fig. 14 we show the differential cross section  $d^2\sigma/dy dp_T$  as a function of the rapidity  $y$  for  $\sqrt{s} = 298 \text{ GeV}$ ,  $\mu = M = M_f = p_T$ , and two different values of  $p_T$ :  $p_T = 5$  and  $10 \text{ GeV}$ . We observe that these distributions are quite symmetric around  $y_{\text{lab}} \sim 2$  and that the NLO corrections to the hard-

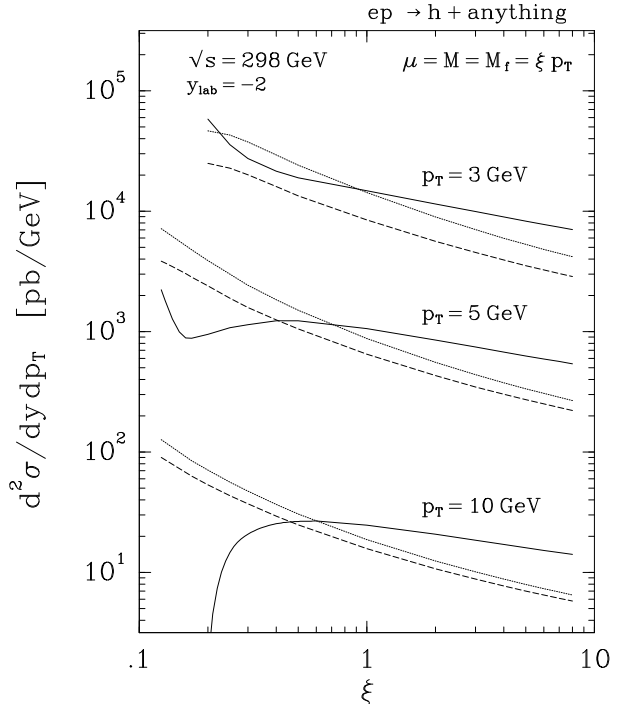


**Fig. 13.** Scale dependence of  $d^2\sigma/dy dp_T$  for the resolved contribution to  $ep \rightarrow hX$  at  $\sqrt{s} = 298 \text{ GeV}$ ,  $y_{\text{lab}} = -2$ , and three different values of  $p_T$ ,  $p_T = 3, 5, 10 \text{ GeV}$ . The solid lines indicate the NLO result, the dotted lines the LO result, and the dashed lines the LO result with structure functions and  $\alpha_s$  at the NLO level

scattering cross section do not change their shape in any significant way.

## 4 Summary and Conclusions

We have presented next-to-leading-order predictions for inclusive single-charged hadron and single- $\pi^0$  production via resolved photoproduction at HERA. We have confronted these predictions with first experimental data from the H1 Collaboration and found that both are in good agreement as for the slope in  $p_T$ . To allow meaningful tests of the QCD-improved parton model and to probe quantitatively the parton structure of the photon, more accurate measurements are needed.

We find that the LO and NLO calculations coincide when the renormalization and factorization scales are chosen to lie just below  $p_T$ . We consider this agreement as accidental, since there is a substantial discrepancy for other choices of scales. As expected, the inclusion of NLO corrections leads to a reduction in the scale dependence of the cross sections. Therefore, within

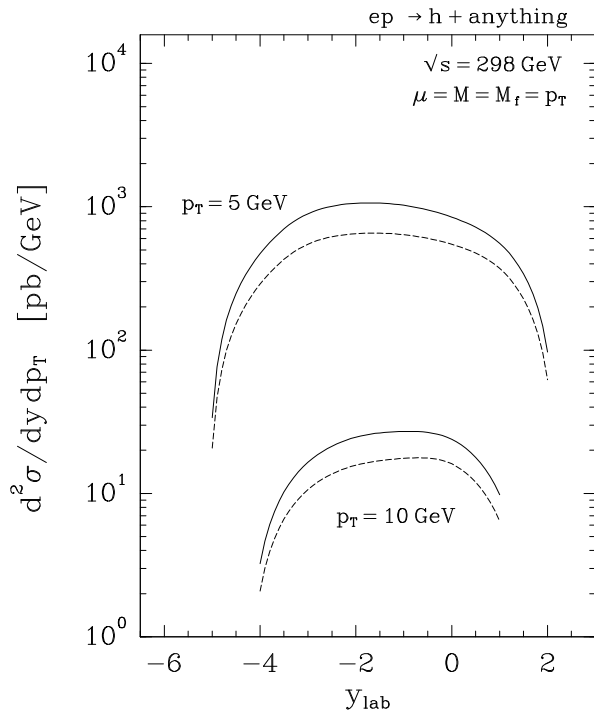


**Fig. 14.** Rapidity distribution of  $d^2\sigma/dy dp_T$  for the resolved contribution to  $ep \rightarrow hX$  at  $\sqrt{s} = 298$  GeV,  $p_T = 5, 10$  GeV. The solid lines indicate the NLO result and the dashed lines the LO result with structure functions and  $\alpha_s$  at the NLO level

the scale variation in NLO, our results can be considered as an absolute prediction for resolved photoproduction of single hadrons in  $ep$  collisions. This is particularly important in the case of  $\pi^0$  production, since such events provide a background for prompt-photon emission. However, precisely in the case of neutral hadrons the fragmentation functions used in our calculation may not be completely reliable.

A further limitation of our analysis is related to the use of LO fragmentation functions. Already now we observe that the dependence on the fragmentation scale is reduced when the NLO terms of the hard-scattering cross section are included. We expect the results to become even more stable when also NLO fragmentation functions are utilized.

Finally, in order to disentangle experimentally resolved and direct photoproduction, it is necessary to select small- $p_T$  hadrons and/or to require the detection of the photon remnant jet. At present, this does not represent a problem, since the data are still being accumulated at relatively low  $p_T$ . However, as soon as data at larger  $p_T$  will become available, the direct process will have to be evaluated in NLO and matched to the calculation presented here.

## Acknowledgments

We thank L. Gordon for useful communications regarding [7].

## References

1. T. Ahmed et al., H1 Coll.: Phys. Lett. B297 (1992) 205
2. M. Derrick et al., ZEUS Coll.: Phys. Lett. B297 (1992) 404
3. J.G. Morfin, W.K. Tung: Z. Phys. C52 (1991) 13
4. A.D. Martin, R.G. Roberts, W.J. Stirling: Phys. Rev. D37 (1988) 1161; Mod. Phys. Lett. A4 (1989) 1135; P.N. Harriman, A.D. Martin, W.J. Stirling, R.G. Roberts: Phys. Rev. D42 (1990) 798; J. Kwiecinski, A.D. Martin, W.J. Stirling, R.G. Roberts: Phys. Rev. D42 (1990) 3645
5. A.D. Martin, W.J. Stirling, R.G. Roberts: Phys. Rev. D47 (1993) 867
6. M. Glück, E. Reya, A. Vogt: Phys. Rev. D45 (1992) 3986; Phys. Rev. D46 (1992) 1973
7. L.E. Gordon, J.K. Storrow: Z. Phys. C56 (1992) 307
8. P. Aurenche et al.: Z. Phys. C56 (1992) 589
9. P. Chiappetta et al.: Preprint CPT-92/PE.2841, ENSLAPP-A-416/93, FNT/T-92/46, IPNL 93-1 (December 1992)
10. R. Baier, J. Engels, B. Petersson: Z. Phys. C2 (1979) 265
11. M. Anselmino, P. Kroll, E. Leader, Z. Phys. C18 (1983) 307
12. F.M. Borzumati, B.A. Kniehl, G. Kramer: Z. Phys. C57 (1993) 595
13. F. Aversa, P. Chiappetta, M. Greco, J.Ph. Guillet: Phys. Lett. B210 (1988) 225; ibid. B211 (1988) 465; Nucl. Phys. B327 (1989) 105
14. C.F. von Weizsäcker, Z. Phys. 88 (1934) 612; E.J. Williams, Phys. Rev. 45 (1934) 729(L)
15. For a review see E. Paul: DESY Report 92-026 (February 1992)
16. H. Baer, J. Ohnemus, J.F. Owens: Z. Phys. C42 (1989) 657
17. K. Charchuła: Comput. Phys. Commun. 69 (1992) 360
18. M. Drees, K. Grassie: Z. Phys. C22 (1985) 451
19. P. Amaudruz et al., New Muon Coll.: Nucl. Phys. B371 (1992) 3; Phys. Lett. B295 (1992) 159; E. Kabuss: in: Proceedings of DESY-Zeuthen Workshop on Deep Inelastic Scattering, 1992
20. S.R. Mishra et al., CCFR Coll.: Columbia University Report, NEVIS #1459 (June 1992)